# New Sensing Technology and New Applications in Geotechnical Engineering

## Nouvelle technologie de détection et nouvelles applications à l'ingénierie géotechnique

Wang Y.H., Ooi G.L., Gao Y.
*Department of Civil and Environmental Engineering, The Hong Kong University of Science and Technology, Hong Kong*

ABSTRACT: Soils are inherently a particulate medium, and relevant physical principles behind the macro-scale engineering properties originate from particle interactions. However, it is difficult in general to conduct measurements which can monitor soil particle movement and even characterize micromechanics behind different soil behaviour. Advancement of sensing technologies in recent years offers us the opportunity to do so. Two examples are presented in this paper. The first is on using the tactile pressure sensor (film-like sensor) to monitor the evolution of contact normal forces among particles in aged sand. The measurement reveals that the contact forces are continuously redistributed during aging. This ultimately strengthens the soil structure and therefore increases the associated small-strain shear modulus. The second is on using the miniature MEMS accelerometer to characterize the soil movement in a laboratory flow landslide. The MEMS sensors demonstrate promising results in describing the rich features of local responses of soil movement in the shear zone, e.g. liquefaction, deceleration, contraction and dilation.

RÉSUMÉ : Les sols sont intrinsèquement un milieu particulaire et les principes physiques pertinents derrière les propriétés mécaniques à macro-échelle proviennent d'interactions entre particules. Cependant, il est difficile en général d'effectuer des mesures qui peuvent suivre le mouvement des particules du sol et même de caractériser la micromécanique derrière différents comportements du sol. L'avancée des technologies de détection ces dernières années nous offre la possibilité de le faire. Deux exemples sont présentés dans cet article. Le premier utilise le capteur de pression tactile pour suivre l'évolution des forces de contact normales entre des particules dans du sable âgé. La mesure révèle que les forces de contact sont continuellement redistribuées au cours du vieillissement. Cela renforce finalement la structure du sol et augmente donc le module de cisaillement associé à petites déformations. Le second utilise l'accéléromètre miniature MEMS pour caractériser en laboratoire le mouvement du sol dans un glissement de terrain. Les capteurs MEMS démontrent des résultats prometteurs pour la description des caractéristiques abondantes des réponses locales du mouvement du sol dans la zone de cisaillement, par exemple, la liquéfaction, la décélération, la contraction et la dilatation.

KEYWORDS: tactile pressure sensor; aging mechanism; MEMS • landslide initiation mechanism.

## 1 INTRODUCTION

Measurements of micromechanical interactions among soil particles are invaluable to constitute insights into the underlying physics of different soil behavior encountered in geotechnical engineering. However, it is difficult in general to conduct measurements which can monitor soil particle movements and even characterize micromechanics involved. In recent years, manufacturing industries witness breakthroughs in both miniaturization of sensors and improvement of sensing technologies. Therefore, we have an opportunity to carry out measurement at the particulate scale. In this paper we would like to introduce two applications in laboratory testing using such new technologies: (1) tactile pressure sensor to characterize the underlying mechanisms of aging in sand, and (2) 3D Micro-Electro-Mechanical-Systems (MEMS) accelerometers to capture soil movement in the initiation process of a laboratory flow landslide.

Aging can occur in all types of soils: for instance, increases in their shear strength and shear modulus are observed as time elapses. Such aging effects in sands have been reported not only from laboratory tests but also via field observations (e.g., see review in Schmertmann 1991, Mitchell and Soga 2005, Wang and Tsui 2009; Gao et al. 2013). Nevertheless, at present, the associated underlying mechanisms remain inconclusive. In the first study, the tactile pressure sensor installed in a tailor-made oedometer was used to characterize the evolution of contact normal force among particles in dry sand during aging. The bender element sets were also utilized in parallel to monitor the associated changes in the small-strain shear modulus, $G_{max}$. The ultimate goal of this experiment is to provide evidence that could account for the underlying mechanisms of aging effects.

Initiation mechanisms of flow landslides are likewise still an unsettled open discussion. There had been published studies linking the initiation process of flow landslides to pore pressure rise and presence of fines in soil (Iverson et al. 2000, Wang and Sassa 2003); however, exactly how the shear zone develops, liquefies or decelerates due to dilation prior to complete fluidization is not measured. The miniature size of 3D MEMS accelerometers (in the range of *mm*) makes the measurements of localized soil responses inside slope possible since they can move like a soil particle without any pronouncing inertial effect. Reported MEMS sensor responses shed lights on a variety of soil movement involved in the initiation process of flow landslide, which will be discussed in detail in the second study.

## 2 USING TACTILE PRESSURE SENSOR FOR THE STUDY OF AGING MECHANISMS

### *2.1 The I-scan system*

Tactile pressure sensors are ultra-thin and flexible and comprise numerous individual tiny sensing elements, called sensels. These features resolve the problems associated with the conventional load cells and enable us to accurately measure stress inside soils. Fig. 1 presents the pressure mapping system used in the first study, i.e., the I-Scan® system (Tekscan Inc., MA., USA). This system consists of software, scanning electronics (called a handle), and a tactile pressure sensor. There are 1936 sensels in the sensor adopted in this study (model 5076). The sensel is a force-sensitive resistor, whose impedance

changes in response to different loading. When a force is applied to the sensor, the analog-to-digital converter assigns a digital output (DO) value between 0 and 255 (i.e., 8-bit resolution) to each sensel, depending on the corresponding impedance value. This DO can then be correlated to the pressure or other engineering units through calibration.

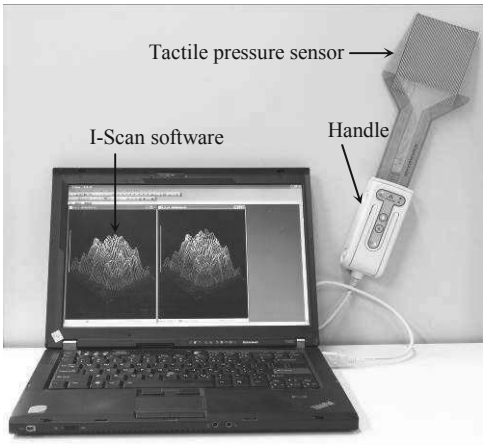


Figure 1. The I-Scan system.

*2.2 Experimental setup and plan*

Fig. 2 presents the experimental setup. A tailor-made oedometer with inner dimensions of 100 × 100 × 40 *mm* was used. Two sets of bender elements were utilized to obtain the small-strain, shear moduli $G_{hv}$ and $G_{hh}$, where the first and second subscripts specify the directions of wave propagation and polarization, respectively; *h* means the horizontal direction and *v* stands for the vertical direction. Each set of bender elements consisted of one source and one receiver. The distance *d* between the source and the receiver is fixed at 80 mm throughout the test. The corresponding shear wave velocity $V_s$ and shear modulus can be derived by $G = \rho(V_s)^2 = \rho(d/t)^2$ where $\rho$ is the soil density. The tactile pressure sensor was put between the upper and bottom box to measure the stress distribution inside soils. The calibration of tactile sensors including the creep (or drift) effect followed the procedure suggested by Gao and Wang (2012). The testing material was dry Leighton Buzzard sand (fraction E).

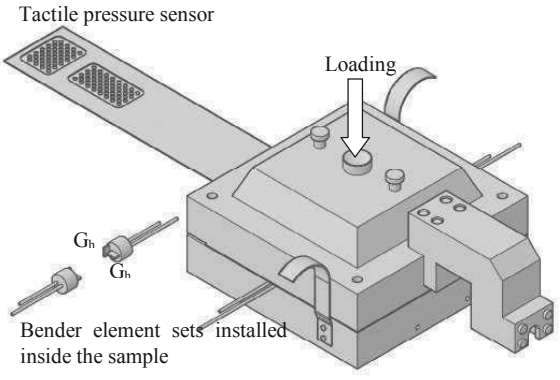


Figure 2. Experimental setup.

During the aging process, the applied vertical stress onto the sand sample was kept constant at $\sigma_v$ =197.21 kPa for three days. The associated shear modulus changes was continuously monitored using the bender element tests and the evolution of contact normal forces among particles was constantly characterized by the tactile pressure sensor and the I-scan system.

*2.3 Experimental results and discussion*

Fig. 3 presents the variations in $G_{hv}$ and $G_{hh}$ during the aging process. The variations are presented in terms of the modulus change, i.e., $(G_t - G_{in})/G_{in}$ where $G_t$ and $G_{in}$ are the moduli at any time *t* and at the initial stage of *t* = 10 min, respectively. As expected, the stiffness continues to increase, suggesting the sample is strengthened during the process of aging. In addition, the increase is greater in $G_{hv}$ than in $G_{hh}$.

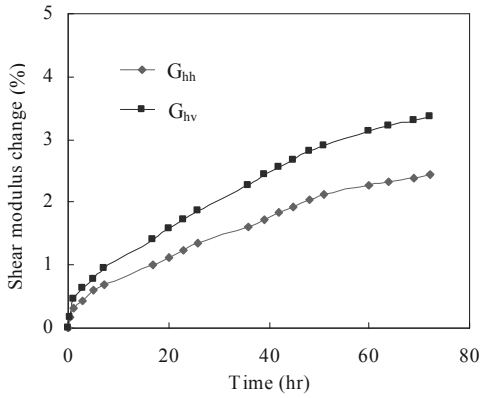


Figure 3. The experimental results of shear modulus changes versus time during three days of aging at $\sigma_v$ = 197.21 kPa.

Fig. 4 shows the probability distributions of measured, normalized contact forces (in the vertical direction, $F_z$) by the tactile pressure sensor before and after three days of aging under $\sigma_v$ = 197.21 kPa. It can be readily seen that the contact forces are redistributed after three days of aging.

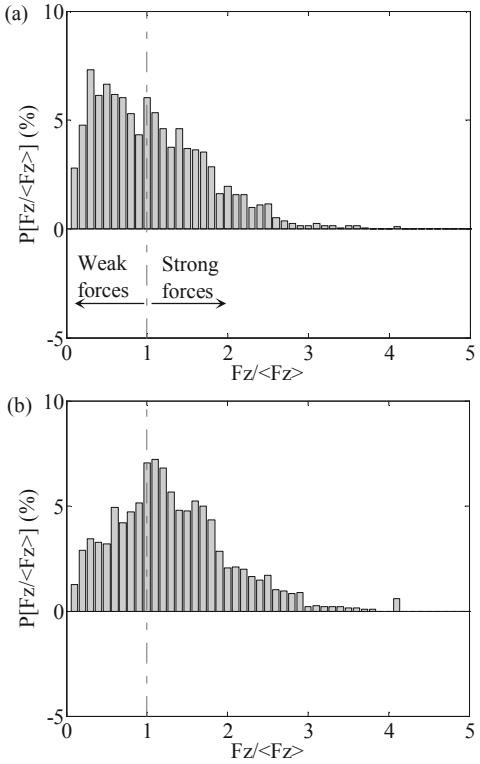


Figure 4 Experimental results of the probability distributions of normalized contact forces at $\sigma_v$ = 197.21 kPa (a) before and (b) after aging.

In order to further discuss such behavior, the contact forces are categorized into two groups, i.e., strong and weak forces. The categorization of strong and weak forces (i.e., the contact normal forces at strong and weak contacts or at strong and weak

networks) follows the suggestion of Radjai et al. (1996). When the normal contact force $F_n$ is greater than its mean $\langle F_n \rangle$ (i.e., $F_n / \langle F_n \rangle > 1$), it is regarded as a "strong" force; otherwise it is a "weak" force. Also found in Fig. 4 is that the probability distributions of weak forces decrease after aging. That is, the force redistribution leads to increasing contact normal forces in the weak force network such that some of the contact normal forces that originally belong to weak ones can be changed to the group of strong forces. In addition, the force distribution becomes more homogenized after aging because the associated coefficient of variation (CV) in $F_z$ reduces from 0.726 to 0.705. Since the weak forces become fewer and the contact forces become more homogenized in the sample, the soil structure is strengthened and so is the associated $G_{hv}$. A comprehensive data set and more detailed explanations with the aid of DEM simulations can be found in Gao (2012) and Gao and Wang (2013).

## 3 USING THE 3D MEMS ACCELEROMETER FOR THE STUDY OF LANDSLIDE INITIATION PROCESS

Micro-Electro-Mechanical-Systems (MEMS) is a classification of devices, as well as the means of fabrication and manufacturing. In 1959, Richard Feynman took the helm of describing the "problem of manipulating and controlling things on a small scale" and thence pioneers like Analog Devices have since miniaturized conventional sensors from the size of a closed fist to that of a quarter of fingernail (Feynman 1959). The MEMS technology allows for batch-wise etching production, thereby minimizing manufacturing cost and at the same time promising standard accuracy and quality across sensors. Up until the recent 5 years only does stabile 3-dimensional MEMS accelerometer become available in the market. The ADXL335 accelerometer model by Analog Devices is selected for the second study to characterize localized soil responses prior to and during landslide initiation.

The Analog Devices' ADXL335 is a miniature accelerometer which measures 4 × 4 × 1.45 *mm* (Length × Width × Thickness) in size and comes at a low price, about couple US dollars per piece. It utilizes low power, typically functioning at 3.0 *V* and 350 $\mu A$. The accelerometer is capable of 3-axis sensing and measures full-scale acceleration within ±3.6 *g* with a frequency bandwidth ranging from 0.5 to 1600 *Hz* for the X and Y axes, and a range of 0.5 to 550 *Hz* for the Z axis. Fig. 5 illustrates the ADXL335 surface mounted on an in-house designed printed circuit board (PCB) since soldering by hand is impossible for the tiny pins; the PCB is 11 × 11 × 2 *mm* (Length × Width × Thickness) in size and the circuitry directs the corresponding pins to larger soldering points. The package was coated with several layers of air-dry polyurethane for waterproof. Also shown in Fig. 5 are the positive directions of X, Y and Z axes. The MEMS accelerometer is attractive not just because of its light-weight, miniature size, low-cost and standardized quality; it also boasts of the unique features of measuring the static acceleration of gravity in tilt-sensing applications, as well as dynamic acceleration resulting from motion, shock or vibration.

These unique features provide us with two kinds of information coming in one package. The DC bias offset in signal conditioned voltage output gives us the tilt angle in reference to the gravity. When the accelerometer is static, we can calculate the current angles of tilt in three dimensions about the accelerometer's center of mass, known as roll, pitch and yaw; when it is in motion, we can calculate the direction of movement by finding the vector sum of the acceleration. In total 10 MEMS accelerometers were installed in both vertical and horizontal array so that dilative or contractive behavior between layers of soil could also be identified.

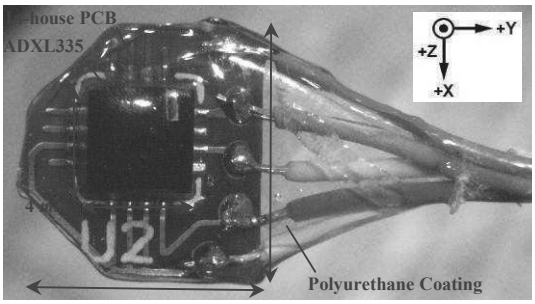


Figure 5. Analog Devices' ADXL335 surface mounted on PCB.

### *3.1 Calibration of 3D MEMS Accelerometer*

All the MEMS accelerometers were connected to a logging computer through National Instruments' NI-USB 6353 analog-to-digital converter with 16-bit resolution. Sampling frequency of every axis was set at 10,000 Hz. Due to batch-wise production, factory performance results of Analog Devices' ADXL335 are compiled from 1000 pieces to determine the mean bias offset value (Analog Devices 2010); however, to further verify whether the sensors we purchased fall within the range as documented, simple calibration using an earthquake shaking table and a high-frequency vibration exciter was carried out. The mean zero bias offset value for X-axis was found to peak at 1.51 V, and for Y and Z axes the value was 1.49 V; all sensors are functioning as detailed in the datasheet. The sensors were also left operating overnight to check for possible noise drift over time. Nothing anomalous happened and the sensors performed normally as documented in the manual. Subsequent conversions from voltage to acceleration which required parameters from the datasheet were cited directly thereafter.

### *3.2 Laboratory Water Flume*

Fig. 6 presents a side view of the well-instrumented laboratory water flume. The rectangular soil prism made of acrylic is of size 100 × 45.2 × 20 cm (Length × Width × Height). A saturation box was affixed at the back to provide standardized antecedent condition before each experiment. In addition to the MEMS accelerometer array (for the positions of accelerometer M1 to M10 see Fig. 6), basal porewater pressure transducers were also installed as indicated by the little squares; a video camera was shooting the process from the top. A layer of bottom porous stone was affixed to the flume rack to provide similar friction angle as the soil specimen at the bottom boundary.

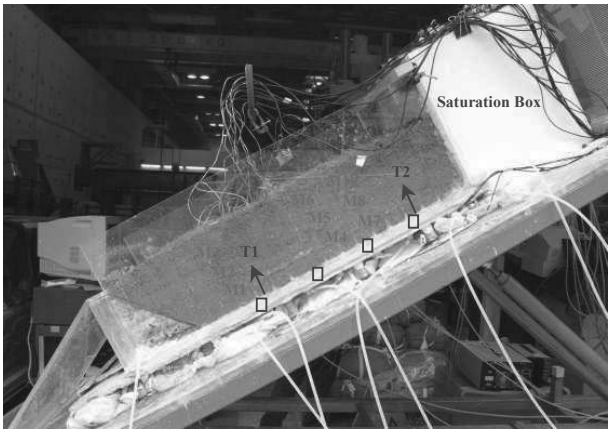


Figure 6. Laboratory water flume setup.

### *3.3 Characterization of Shear Zone Behavior with MEMS*

In this section, we will demonstrate qualitative results from one of the water flume tests set out to investigate how shear zone liquefaction evolves in loose slope without any fines present. MEMS accelerometer M8 situated right within the shear zone in the rear middle of the soil mass was selected to illustrate the landslide mechanism (see Fig. 6). The loose slope was saturated by slow and little groundwater inflow at start, and a fixed interval later a sudden rise of groundwater inflow twice the original volume was first invoked at the bottom of the slope toe (indicated by T1 in Fig. 6); minutes later the rear bottom (T2 in Fig. 6). Both groundwater supply events are also indicated by vertical black lines in Fig. 7.

There are in total 3 sliding events recorded and their occurrence instances are punctuated by the vertical red lines in Fig. 7. The groundwater supply T1 at the slope bottom induced an abrupt liquefaction; inside the shear zone, Y axis of M8 registered a huge contraction and the Z-axis tracked a rotation towards the back then a forward charging jerk. However, the movement of the soil mass ceased as sudden as the initiation; the basal porewater pressure transducer tells us that the porewater pressure built up just then was dissipated. Although by now the groundwater supply T2 at the rear bottom was invoked, the soil mass did not exhibit any noticeable activity, a stark contrast to the loose slope with fines experiment in which complete fluidization occurred by the moment when T2 was invoked. Subsequently what we observed was replenishment of porewater pressure right before sliding event L2 happened and stopped almost instantaneously again; however, this time Y axis of M8 recorded a dilation instead. The porewater pressure abated after L2 then was built up again and finally the whole soil mass fluidized, initiating event L3. The movement was slow; it took 23.9 seconds in total to slide out of the flume. The activity inside shear zone as captured by M8 was a slow dilating rotation, upward and forward as the soil slowly discharged out.

In short, the MEMS accelerometers demonstrated promising results in describing the rich features of sliding events, including local responses of soil movement in the shear zone, e.g. contractions, dilations and the rolling components.

## 4 CONCLUSION

Two new sensing technologies (sensors) were successfully utilized in this paper to reveal aging mechanisms and to monitor local soil movement in a flow landslide event. Using the tactile pressure sensor allows us to measure the contact forces among soil particles and therefore is able to obtain experimental evidence that can explain the underlying mechanisms of aging effects. During aging the contact forces continue to be redistributed. This ultimately leads to increasing contact normal forces in the weak force network such that some of the contact normal forces that originally belong to weak ones can be changed to the group of strong forces. In addition, the force distribution becomes more homogenized. As a result, the soil structure is strengthened and so is the associated small-strain shear modulus.

Because of its miniature size and high sensitivity, the MEMS sensor is allowed to be buried in a laboratory slope to characterize the features of soil movement inside the shear zone during a flow landslide event, such as liquefaction, deceleration, contraction and dilation. All of these observations complement theoretical work and provides us insights into the initiation mechanisms of a flow landslide.

## 5 ACKNOWLEDGEMENTS

This research was supported by the Hong Kong Research Grants Council (GRF 621109 and 620310).

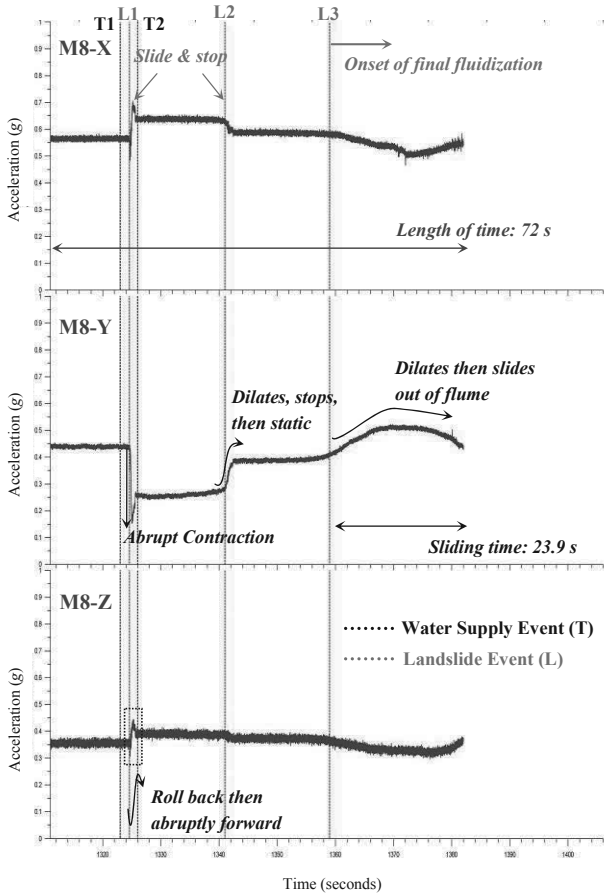


Figure 7. Characterization of sliding features within shear zone in loose slope without fines captured by MEMS accelerometer M8, demonstrating a gradual failure mode.

## 6 REFERENCES

Feynman, R. 1959. *There's plenty of room at the bottom*. URL: http://www.zyvex.com/nanotech/feynman.html

Gao Y. 2012 Experimental characterizations and DEM simulations of aging, creep and structuration in sand. Ph.D. Thesis. The Hong Kong University of Science and Technology.

Gao Y. and Wang Y.H. 2012. Calibration of tactile pressure sensors for measuring stresses in soils. *Tentatively accepted by Geotech. Test. J. ASTM*.

Gao Y. and Wang Y.H. 2013. The underlying mechanism of aging effects on changing sand stiffness. Submitted to Canadian Geotechnical Journal.

Gao Y., Wang Y.H., and Su J.C.P. 2013. Mechanisms of aging-induced modulus changes in sand under isotropic and anisotropic loading. *J. Geotech. Geoenviron. Eng.* (Accepted for publication, http://dx.doi.org/10.1061/(ASCE)GT.1943-5606.0000772).

Iverson, R.M., Reid, M.E., Iverson, N.R., LaHusen, R.G., Logan, M., Mann, J.E. and Brien, D.L. 2000. Acute sensitivity of landslide rates to initial soil porosity. *Science*, 290:513-516.

Mitchell, J. K. and Soga, K. 2005. *Fundamentals of Soil Behavior*, 3rd edition, John Wiley & Sons, Inc., New York.

Radjai, F., Jean, M., Moreau, J.J., and Roux, R. 1996. Force Distributions in Dense Two-Dimensional Granular Systems. *Phys. Rev. lett.*, 77(2), 274-277.

Schmertmann, J.H. (1991). The mechanical aging of soils. *J. Geotech. Engrg., ASCE*, 117(9): 1286-1330.

Wang, G. and Sassa, K. (2003). Pore-pressure generation and movement of rainfall-induced landslides: effects of grain size and fine-particle content. *Eng. Geol.*, 69, 109-125.

Wang, Y.H. and Tsui, K.Y. 2009. Experimental characterization of dynamic property changes in aged sands. *J. Geotech. Geoenviron. Eng., ASCE*, 135(2), 259-270.